Synthesis of BaTiO$_3$-TiO$_2$-Graphene Nanocomposites and Kinetics Studies on their Photocatalytic Activity

J. Li[1], J.W. Ko[1], W.B. Ko[1,2*]

[1]Department of Convergence Science, Graduate School, Sahmyook University, Seoul 139-742, South Korea
[2]Department of Chemistry, Sahmyook University, Seoul 139-742, South Korea

Article info

Abstract

BaTiO$_3$-TiO$_2$ nanoparticles were fabricated by a wet-chemical method using barium chloride dihydrate (BaCl$_2$·2H$_2$O), titanium dioxide (TiO$_2$), and oxalic acid (C$_2$H$_2$O$_4$) as precursors. BaTiO$_3$-TiO$_2$-graphene nanocomposites were obtained by heating the BaTiO$_3$-TiO$_2$ nanoparticles with graphene in an electric furnace at 700 °C for 2 h. X-ray diffraction analysis revealed that the resulting products were BaTiO$_3$-TiO$_2$-graphene nanocomposites. Scanning electron microscopy revealed the morphology of the nanocomposites. UV-vis spectrophotometry was used to analyze the photocatalytic degradation of several organic dyes using the BaTiO$_3$-TiO$_2$-graphene nanocomposites as a photocatalyst under ultraviolet irradiation at 254 nm.

1. Introduction

Because of the unique electrical, optical, magnetic, and catalytic properties of nanosized materials, many researchers have focused on the development of various new nanomaterials with good performance and fine grain sizes [1–3].

Barium titanate (BaTiO$_3$), an alkaline earth titanate with a cubic perovskite structure, possesses excellent dielectric, ferroelectric, and piezoelectric properties that make it one of the most important materials used in multilayer ceramic capacitors and optoelectronic devices [4–7]. Over the past decade, extensive investigations have been carried out to synthesize different BaTiO$_3$ nanostructures such as nanoparticles, nanowires, and nanoplates [8–10]. In addition, many alternative methods such as hydrothermal treatment [11, 12], sol-gel processing [13], solvothermal methods [14], microwave synthesis [15], and solid-state reactions of oxides [16, 17] have been successfully used to prepare BaTiO$_3$ nanopowders. Conventionally, BaCO$_3$ and TiO$_2$ have been used as raw materials in solid-state reactions in order to obtain BaTiO$_3$ [18]. However, the decomposition of BaCO$_3$ at high temperatures (above 1200 °C) can easily lead to agglomeration [7].

Recently, many researchers have synthesized BaTiO$_3$ using hydrothermal treatment methods. The resulting products obtained via hydrothermal synthesis have narrow size distributions and lower calcination temperatures compared to those obtained via solid-state reactions [19]. Moreover, microwave-assisted synthesis is known as an effective method to prepare uniformly sized BaTiO$_3$ nanoparticles [20].

Photocatalytic water splitting is a possible solution to the problem of increasing energy demand, and is therefore appealing to researchers [21, 22]. Over the past few years, many efficient photocatalysts have been fabricated. Semiconductors such as ZnO [23], TiO$_2$ [24], and CdS [25] can be sensitized by organic dyes and have shown excellent activity in the photocatalytic degradation of organic dyes.

This is due to the binding energy provided by the empty conduction band and filled valence band of the semiconductor [26]. Although many photocatalysts have been investigated and applied for the removal of dye pollutants, an efficient photocatalyst with high stability is still needed. Graphene as an allotrope of carbon atom with two-dimensional honeycomb lattice has been studied in many fields for its unique properties [27-31]. Graphene displayed remarkable electron mobility and has a great application prospect in the electronic device and various kinds of photocatalyst [32].

In this paper, we present the synthesis of BaTiO$_3$-TiO$_2$ nanoparticles using barium chloride

dihydrate (BaCl$_2$·2H$_2$O) and titanium dioxide (TiO$_2$) as precursors, via a wet-chemical method.

In addition, BaTiO$_3$-TiO$_2$-graphene nanocomposites were prepared by the calcination of BaTiO$_3$-TiO$_2$ nanoparticles and multilayered graphene in an electric furnace. X-ray diffractometry (XRD) and scanning electron microscopy (SEM) were used to characterize the resulting products. In photocatalytic studies, the BaTiO$_3$-TiO$_2$-graphene nanocomposites used for the degradation of organic dyes such as methylene blue (MB), rhodamine B (RhB), brilliant green (BG), and methyl orange (MO) under 254 nm ultraviolet (UV) light irradiation.

2. Experimental

2.1. Materials and instruments

Barium chloride dihydrate [BaCl$_2$·2H$_2$O], titanium (IV) oxide [anatase TiO$_2$], oxalic acid dihydrate [C$_2$H$_2$O$_4$·2H$_2$O], nitric acid [HNO$_3$], MB, RhB, and tetrahydrofuran (THF) were obtained from Samchun Chemicals (Korea). BG and MO were purchased from Sigma-Aldrich (India), and graphene was supplied by ENano Tec.

Microwave irradiation was performed in a domestic oven at the maximum power (2450 MHz, 700 W). An electric furnace (Ajeon Heating Industy Co., Ltd) was used for heating the samples at 700 °C for 2 h. The structures of the products were characterized by XRD (Bruker, D8 Advance). SEM observation (JEOL Ltd, JSM-6510) at an accelerating voltage of 0.5 to 30 kV was performed to examine the surface morphology of the products. Photocatalytic degradation was performed using a UV lamp (8 W, 254 nm, 77202 Marne La Valee-cedex 1 France) and characterized using a UV-vis spectrophotometer (Shimazu UV-1619 PC).

2.2. Synthesis of BaTiO$_3$-TiO$_2$-graphene nanocomposites

BaCl$_2$·2H$_2$O (0.05 mol) and TiO$_2$ (0.05 mol) powders used as starting materials were dispersed into 100 ml of a 0.5 M oxalic acid solution. After the solution was stirred for 4 h at 70 °C, the mixture was subjected to microwave irradiation for 6 min (30 s, 12 times). After allowing the mixture to stand for 5 min, the supernatant was poured into a beaker, and the precipitate was washed 5 times with distilled water and dried in an electric oven at 100 °C for 12 h. After it had dried, the precipitate was ground into a powder with a mortar and pestle. The powder was heated at 700 °C for 2 h in an argon atmosphere

to form BaTiO$_3$-TiO$_2$ nanoparticles. In order to remove the byproduct BaCO$_3$, the powder was stirred for 30 min in 200 ml of a 1 M HNO$_3$ solution at 70 °C. The BaTiO$_3$-TiO$_2$ nanoparticles were then obtained *via* washing and drying. The final product, BaTiO$_3$-TiO$_2$-graphene nanocomposites, were obtained by heating the BaTiO$_3$-TiO$_2$ nanoparticles and graphene mixed in tetrahydrofuran with a mass ratio of 1:1 at 700 °C for 2 h under an atmosphere of inert argon gas.

2.3. Characterization of BaTiO$_3$-TiO$_2$-graphene nanocomposites

The XRD pattern of the BaTiO$_3$-TiO$_2$-graphene nanocomposites was obtained using powder X-ray diffraction with Cu Kα radiation ($\lambda = 1.54178$ Å).

The crystalline phases of the nanocomposites were identified on the basis of the XRD peaks. The morphologies and shapes of the particles in the sample were observed by SEM.

2.4. Evaluation of photocatalytic activity

The photocatalytic activity of the BaTiO$_3$-TiO$_2$-graphene nanocomposites was evaluated by investigating the degradation of organic dyes such as MB, RhB, BG, and MO. A 5 mg sample of the BaTiO$_3$-TiO$_2$-graphene nanocomposites was added to a reactor along with 10 ml of organic dye solution. After absorption in a dark environment for 30 min, the organic dye solution and photocatalyst were irradiated in the reactor by a UV lamp at a wavelength of 254 nm. The distance between the reactor and the lamp was 1 cm. The entire process of photocatalytic degradation was analyzed using a UV-vis spectrophotometer.

3. Results and Discussion

3.1. Crystal structure and morphology of BaTiO$_3$-TiO$_2$-graphene nanocomposites

Figure 1 shows the XRD patterns indicative of the crystal structure of the BaTiO$_3$-TiO$_2$-graphene nanocomposites. Peaks were observed at 2θ values of 22.3°, 31.7°, 39.1°, 45.3°, 56.3°, and 65.9°, which could be indexed to the (100), (110), (111), (200), (211), and (220) crystal planes of BaTiO$_3$ possessing a cubic structure, respectively (JCPDF 31-0174) [31, 32]. The peaks located at 2θ values of 25.5°, 38.0°, 48.2°, 54.1° and 54.9° were attributed to the (101), (004), (200), (105), and (211) planes of anatase TiO$_2$ (PDF card 21-1272, JCPDS) [26]. The

diffraction peak of graphene was determined to be at about $2\theta = 26.8°$. The crystallite size was calculated by using Scherrer's formula from the full-width at half maximum (FWHM) of the XRD peaks [31]. The formula can be written as follows:

$$D = \frac{K\lambda}{\beta \cdot COS\theta}$$

where K is the shape factor taken as 0.9, λ is the wavelength of the Cu Kα radiation ($\lambda = 1.54178$ Å) used in the powder XRD analysis, β is the FWHM, and 2θ is the angle between the incident and scattered X-rays.
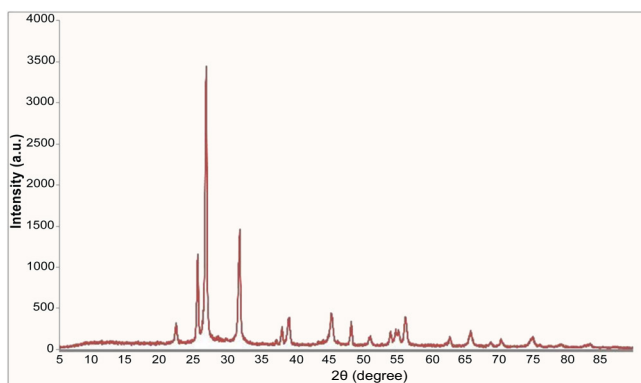

Fig. 1. XRD pattern of the $BaTiO_3/TiO_2$-graphene nanocomposites.

Table 1 shows the estimated FWHM of the XRD peaks and the crystalline size of the $BaTiO_3$ nanoparticles. The mean crystalline size of the $BaTiO_3$ nanoparticles was calculated to be 18.12 nm.

Table 1
Structural parameter calculation of $BaTiO_3$ nanoparticles

hkl	2θ (degree)	Intensity	FWHM 2θ (degree)	Crystallite size (nm)
100	22.3305	323	0.4136	19.59
110	31.7245	1467	0.3544	23.32
111	39.0506	394	0.5120	16.47
200	45.2935	443	0.5908	14.58
211	56.2827	401	0.5121	17.60
220	65.9129	231	0.5514	17.18

By analyzing the XRD peaks due to anatase TiO_2, the data shown in Table 2 were obtained, and the average crystalline size of TiO_2 in the $BaTiO_3$-TiO_2-graphene nanocomposites was determined to be 23.06 nm.

Additionally, the single (200) diffraction peak with no splitting at around $2\theta = 45°$ indicated that $BaTiO_3$ nanoparticles with the cubic and tetragonal phase were obtained [19, 33, 34].

Table 2
Structural parameter calculation of TiO_2 nanoparticles

hkl	2θ (degree)	Intensity	FWHM 2θ (degree)	Crystallite size (nm)
101	25.5209	1165	0.2757	29.57
004	38.0068	279	0.3545	23.72
200	48.2279	341	0.3545	54.57
105	54.1163	222	0.4333	20.60
211	54.8844	248	0.5321	16.84

Figure 2 shows the SEM image of the $BaTiO_3$-TiO_2-graphene nanocomposites.

As shown in Fig. 2, the $BaTiO_3$-TiO_2 nanoparticles have a spherical and stone-like morphology, and the particles gather together. Compared with the $BaTiO_3$-TiO_2 nanoparticles, lamellar graphene appeared to have a littery morphology in the SEM image. Additionally, the $BaTiO_3$-TiO_2 nanoparticles were surrounded by the graphene sheet or adhered to its surface.
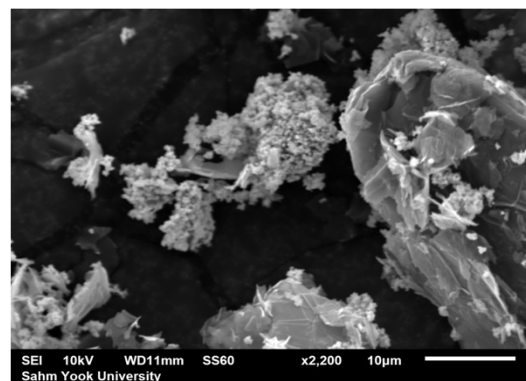

Fig. 2. SEM image of the $BaTiO_3/TiO_2$-graphene nanocomposites.

3.2. Photocatalytic activity of $BaTiO_3$-TiO_2-graphene nanocomposites for organic dye degradation

Figure 3 shows the UV-vis absorption spectra for the degradation of organic dyes using the $BaTiO_3$-TiO_2-graphene nanocomposites as a photocatalyst. A 10 mL vial was used as a reactor, and photocatalytic degradation of the organic dyes was performed in an aqueous medium.

The dye concentration was controlled by maintaining the initial absorbance at 1.0 and the concentration of the $BaTiO_3$-TiO_2-graphene nanocomposites was controlled at 500 mg/L. The reactor was placed in a dark environment for 30 min as soon as the $BaTiO_3$-TiO_2-graphene nanocomposites were added to the organic dye solution. Then, a UV lamp with wavelength of 254 nm was used to irradiate the

reactor for 10 min. As a result, the color of the organic dyes changed from dark to light and the intensity of the absorbance of the organic dyes decreased with an increase in the irradiation time. In BaTiO$_3$-TiO$_2$-graphene nanocomposites, graphene was acted on as good electron acceptors can accept the electrons by UV light irradiation and the electrons excited in conduction band of BaTiO$_3$ are transferred to the surface of grapheme [30, 35, 36]. Therefore, the life-time of the excited electrons (e$^-$) and holes (h$^+$) is prolonged in the process, including a higher quantum efficiency. The electrons can react with O$_2$ to generate ·O$_2^-$, and the holes migrate to the surface and react with OH$^-$ to generate OH·, these radicals can react with adsorbed pollutants. BaTiO$_3$-TiO$_2$-graphene nanocomposites performed better as a photocatalyst, compared to BaTiO$_3$, TiO$_2$, BaTiO$_3$-TiO$_2$, itself [26, 37, 38].

This can be seen in Fig. 3a, which shows the degradation of MB using the BaTiO$_3$-TiO$_2$-graphene nanocomposites as a photocatalyst. Figure 3b shows the UV-vis spectra for the degradation of BG. Figure 3c shows the degradation of RhB in the presence of the BaTiO$_3$-TiO$_2$-graphene nanocomposites, while Fig. 3d shows the UV-vis spectra for the degradation of MO. The photocatalytic activity was superior for BG when compared with that for MB, RhB, and MO.

3.3. Kinetics of photocatalytic degradation of organic dyes

In this work, we investigated the kinetics of photocatalytic degradation of organic dyes such as MB, BG, RhB, and MO using the Langmuir-Hinshelwood model [39]. The equation can be written as follows:

$$ln\ (C/C_0) = -\ K\alpha\rho \cdot t$$

where C_0 is the initial concentration of the organic dye solution and C is the concentration at the measurement time t. $K\alpha\rho$ is the apparent reaction rate constant. As shown in the Fig. 4, the degradation of the organic dyes followed a pseudo-first-order rate law. Also, Fig. 4 shows that the order of the kinetics for the photocatalytic degradation of the organic dyes was BG > RhB > MB > MO. This means that the degradation of BG was the fastest and that of MO was the slowest in the presence of the BaTiO$_3$-TiO$_2$-graphene nanocomposites under UV irradiation at 254 nm.
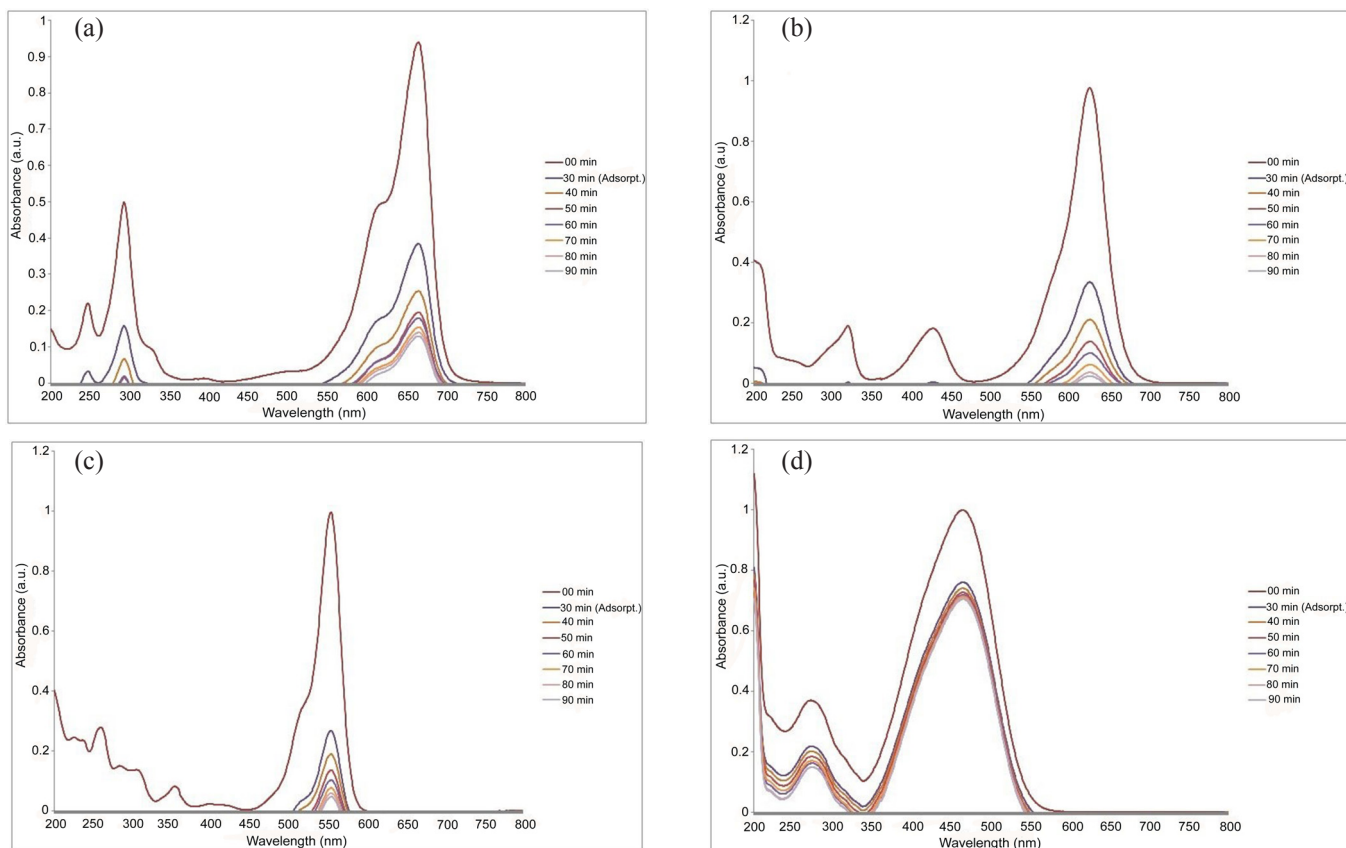

Fig. 3. UV-vis spectra for the degradation of (a) MB, (b) BG, (c) RhB, and (d) MO using the BaTiO₃/TiO₂-graphene nanocomposites as a photocatalyst under UV irradiation at 254 nm.
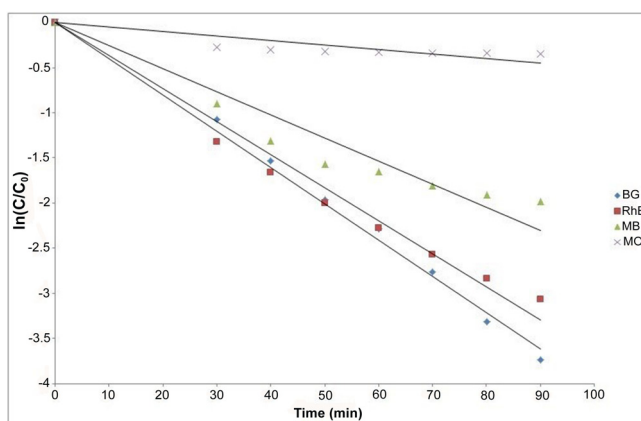
Fig. 4. Kinetics study for the photocatalytic degradation of the organic dyes using the BaTiO$_3$/TiO$_2$-graphene nanocomposites as a photocatalyst.

4. Conclusions

BaTiO$_3$-TiO$_2$ nanoparticles were synthesized using a wet-chemical method. Then, via calcination of these nanoparticles with graphene, BaTiO$_3$-TiO$_2$-graphene nanocomposites were obtained, which exhibited good photocatalytic activity for the degradation of organic dyes like BG, MB, MO, and RhB. XRD patterns showed that BaTiO$_3$ nanoparticles have a completely crystalline structure, with a cubic and tetragonal phase. The crystallite sizes of BaTiO$_3$ and TiO$_2$ in the BaTiO$_3$-TiO$_2$-graphene nanocomposites were calculated by applying Scherrer's formula to the XRD patterns. Morphological characterizations were performed using SEM imaging. Spherical and stone-like BaTiO$_3$-TiO$_2$ nanoparticles were gathered together and were surrounded by the graphene sheet or were stuck to the surface of graphene, as seen in the SEM images. The degradation experiments on BG, MB, MO, and RhB showed that the BaTiO$_3$-TiO$_2$-graphene nanocomposites have good photodegradation efficiency. Kinetics studies of the photocatalytic degradation of the dyes using the BaTiO$_3$-TiO$_2$-graphene nanocomposites were performed using the Langmuir-Hinshelwood model. The rates of photocatalytic degradation of the organic dyes were in the following order: BG > RhB > MB > MO. The results indicate that the photodegradation rate of BG was the highest among those of the other organic dyes in this experiment.

Acknowledgements

References

[1]. M.G. Lines, J. Alloy. Compd. 449 (2008) 242–245.
[2]. S. Sen, R.N.P. Choudhary, P. Pramanik, Mater. Lett. 58 (2004) 3486–3490.
[3]. S. Yoon, J. Dornseiffer, T. Schneller, D. Hennings, S. Iwaya, C. Pithan, R. Waser, J. Eur. Ceram. Soc. 30 (2010) 561–567.
[4]. Y. Hotta, K. Tsunekawa, T. Isobe, K. Sato, K. Watari, Mat. Sci. Eng. A-Struct 75 (2008) 12–16.
[5]. X. H. Ren, Y.K. Cheng, J. Magn. Magn. Mater. 393 (2015) 293–296.
[6]. M. Saleem, J.S. Song, S.J. Jeong, M.S. Kim, S. Yoon, I.S. Kim, Mater. Res. Bull. 64 (2015) 380–384.
[7]. H. Hsiang, Y.L. Chang, J.S. Fang, F.S. Yen, J. Alloy. Compd. 509 (2011) 7632–7638.
[8]. X. Yang, Z. Ren, G. Xu, C. Chao, S. Jiang, S. Deng, G. Shen, X. Wei, G. Han, Ceram. Int. 40 (2014) 9663–9670.
[9]. X. Wei, G. Xu, Z. Ren, Y. Wang, G. Shen, G. Han, J. Am. Ceram. Soc. 91 (2008) 315–318.
[10]. M.T. Buscaglia, C. Harnagea, M. Dapiaggi, V. Buscaglia, A. Pignolet, P. Nanni, Chem. Mater. 21 (2009) 5058–5065.
[11]. M. Saleem, I.S. Kim, J.S. Song, S.J. Jeong, M.S. Kim, S. Yoon, Ceram. Int. 40 (2014) 7329–7335.
[12]. A. Testino, V. Buscaglia, M.T. Buscaglia, M. Viviani, P. Nanni, Chem. Mater. 17 (2005) 5346–5356.
[13]. N. Maso, H. Beltran, E. Cordoncillo, A.A. Flores, P. Escribano, D.C. Sinclair, J. Mater. Chem. 16 (2006) 3114–3119.
[14]. C. Bi, M. Zhu, Q. Zhang, Y. Li, H. Wang, Mater. Chem. Phys. 126 (2011) 596–601.
[15]. S.H. Jhung, J.H. Lee, J.W. Yoon, Y.K. Hwang, J.S. Hwang, S.E. Park, Mater. Lett. 58 (2004) 3161–3165.
[16]. S. Su, R. Zuo, D. Lv, J. Fu, Powder Technol. 217 (2012) 11–15.
[17]. U. Manzoor, D.K. Kim, J. Mater. Sci. Technol. 23 (2007) 655–658.
[18]. V.P. Pavlovic, B.D. Stojanovic, V.B. Pavlovic, Z.M. Stanojevic, Lj. Zivkovic, M.M. Ristic, Sci. Sinter. 40 (2008) 21–26.
[19]. H. Xu, M. Zeng, Asian J. Chem. 27 (2015) 425–428.
[20]. V. Swaminathan, S.S. Pramana, T.J. White, L. Chen, R. Chukka, R.V. Ramanujan, ACS Appl. Mater. Inter. 2 (2010) 3037–3042.
[21]. S.Z. Kang, L. Chen, X. Li, J. Mu, Appl. Surf. Sci. 258 (2012) 6029–6033.
[22]. Z. Li, Y. Teng, L. Xing, N. Zhang, Z. Zhang, Mater. Res. Bull. 50 (2014) 68–72.
[23]. M.A. Behnajady, N. Modirshahla, R. Hamzavi, J. Hazard. Mater.133 (2006) 226–232.
[24]. R. Li, Y. Jia, N. Bu, J. Wu, Q. Zhen, J. Alloy. Compd. 643 (2015) 88–93.
[25]. M.C. Liu, L.Z. Wang, G.Q. Lu, X.D. Yao, L.J. Guo, Energy Environ. Sci. 4 (2011) 1372–1378.

[26]. R. Li, Q. Li, L. Zong, X. Wang, J. Yang, Electrochim. Acta 91 (2013) 30–35.

[27]. L.Y. Lin, D.E. Kim, W.K. Kim, S.C. Jun, Surf. Coat. Tech. 205 (2011) 4864–4869.

[28]. Z. Mansurov, F. Sultanov, S.S. Pei, S. C. Chang, S. Xing, F. Robles-Hernandez, Y.W. Chi, K.P. Huang, Microwave Plasma Enhanced CVD Graphene-Based Aerogels: Synthesis and Study. Proc. Annual World Conf. Carbon (Carbon-2015), Dresden, Germany, p.232.

[29]. F.R. Sultanov, S.S. Pei, M. Auyelkhankyzy, G. Smagulova, B.T. Lesbayev, Z.A. Mansurov, Eurasian Chemico-Technological Journal. 16 (2014) 265–269.

[30]. Z.D. Meng, L. Zhu, T. Ghosh, C.Y. Park, K. Ullah, V. Nikam, W.C. Oh, B. Kor. Chem. Soc. 33 (2012) 3761–3766.

[31]. R. Sengodan, B.C. Shekar, S. Sathish, Optik 125 (2014) 4819–4824.

[32]. W. Li, Z. Xu, R. Chu, P. Fu, J. Hao, J. Alloy. Compd. 482 (2009) 137–140.

[33]. E. Chavez, S. Fuentes, R. A. Zarate, L. P. Campos, J. Mol. Struct. 984 (2010) 131–136.

[34]. W. Wang, L. Cao, W. Liu, G. Su, W. Zhang, Ceram. Int. 39 (2013) 7127–7134.

[35]. G. Williams, B. Seger, P.V. Kamat, ACS Nano 2 (2008) 1487–1491.

[36]. I.V. Lightcap, T.H. Kosel, P.V. Kamat, Nano Lett. 10 (2010) 577–583.

[37]. X.P. Lin, J.C. Xing, W.D. Wang, Z.C. Shan, F.F. Xu, F.Q. Huang, J. Phys. Chem. C 111 (2007) 18288–18293.

[38]. Q.Y. Li, R.Li, L.L. Zong, J.H. He, X.D. Wang, J.J. Yang, Int. J. Hydrogen Energ. 38 (2013) 12977–12983.

[39]. K. Dai, G. Dawson, S. Yang, Z. Chen, L. Lu, Chem. Eng. J. 191 (2012) 571–578.